Design of a Magnet for the Spin-Rotator Device for the High Magnetic Field μSR Instrument at Paul Scherrer Institute

V. Vranković, A. Gabard, I. Meier, R. Stutz, R. Deckardt, S. Sanfilippo, R. Scheuermann, K. Sedlak, D. Reggiani, K. Deiters, T. Rauber, P. Kaufmann, and H. Walther

***Abstract*—In this work we present the design, the construction and the measurements of the magnet for a so-called spin-rotator (Wien filter), a beam line device used to rotate the spin direction (and the associated magnetic moment) of muons in a beam used for condensed matter research at the Swiss Muon Source at the Paul Scherrer Institute. The design parameters – originating both from the properties of the preferred particle beam as well as the technological constraints for the high-voltage components generating the necessary electric field - were optimised for device compactness, cost and high beam transmission.**

***Index Terms*—Wien filter, ExB cross-field device, spin-rotator, Swiss Muon Source, muon beam line, muon spin rotation, magnet design, optimisation, split-pole magnet, beam ray-tracing, beam transmission, Hall probe magnetic measurements.**

I. INTRODUCTION

THE Laboratory for Muon-Spin Spectroscopy (LMU) presently operates six muon spin rotation/relaxation (μSR) instruments at the Swiss Muon Source (SμS) at the Paul Scherrer Institute (PSI) in Switzerland for fundamental studies of magnetic properties of condensed matter, using continuous muon beams. A fully polarized muon acts as a microscopic magnetometer to measure the local magnetic field and its distribution and fluctuations on an atomic length scale [1]. These instruments are used for in-house research and are accessible to external users from an international community through a peer-review proposal system.

The new High Magnetic Field μSR facility [2] is expected to go into operation at the end of 2011. This world-wide unique instrument will allow to study a previously inaccessible range in the B-T phase diagram of condensed matter up to 9.5 T and down to ~20 mK. The main components of the spectrometer are:

i) a high-homogeneity/short length superconducting magnet with active shimming (manufactured by Oxford Instruments [3]),
ii) a fast-timing detector system based on scintillator-readout by Geiger-mode avalanche photodiodes [4], [5],
iii) a dilution refrigerator for fully horizontal operation (manufactured by BlueFors [6], 0.02-20 K) and
iv) a liquid helium flow cryostat (3-320 K).

Manuscript received September 9, 2011.
All the authors are with the Paul Scherrer Institute, Villigen, Switzerland (e-mail: vjeran.vrankovic@psi.ch).

The spectrometer is optimised for measurements of the muon spin rotation, with the muon spin direction (and the associated magnetic moment) perpendicular to the applied magnetic field. The momentum of the muon beam is ~28 MeV/*c*. This beam has to be injected parallel into a magnetic field applied on the target in order not to be deflected by the Lorentz force. Therefore, the spin of an originally fully longitudinally polarized muon beam (created from the pion decay on a muon production target at the SμS) must be rotated by 90°. This rotation is achieved by a beam line device called 'spin-rotator'. This device provides crossed electric and magnetic fields, both applied perpendicular to each other and to the muon's momentum. Simultaneously to rotating the spin, it also acts as a velocity filter (Wien filter) and separates the muons from other particles contaminating the muon beam (mainly positrons).

The design parameters for the spin-rotator device originate from the preferred properties of the muon beam used to study the properties of the target in the spectrometer. Based on experience with other high-voltage devices at PSI (e.g., for the design of vacuum feedthroughs) and technological standards, the maximum supply voltage for the device was chosen to be ± 200 kV, with an operating voltage of ± 175 kV. The gap between the two electrodes has to be as large as possible for maximum transmission, and the length of the electrodes short. A good compromise was found choosing a distance of 120 mm for the electrode gap, and 1800 mm for the effective length. The matching magnetic field for the operating voltage then is ~38 mT. A device with these parameters leads to a spin rotation of 45°, therefore two identical devices in series are required, with a refocusing quadrupole triplet in between.

Because of the complexity of the system (high-voltage technology, electric and magnetic field matching, vacuum, control system) and in order to ensure compatibility with PSI standards, the decision was made to use PSI expertise and design the whole device at PSI. Commercially available components were used whenever possible. A detailed description of the full system will be given elsewhere. This publication will focus on the magnetic part.

II. DESIGN

A. Pole Profile Across the Muon Beam

Given the dimensions of the required vacuum tank that houses the high-voltage electrodes, the magnet for the spin-rotator was designed to have flat poles. A preliminary 2D study based on calculations made by POISSON [7] showed the size advantage of this choice over a magnet with curved poles. With similar field homogeneity (below 1% in the 'good field' region of R=60 mm) and field magnitude (10 mT) in the specified free aperture, a magnet with flat poles is more compact, simpler to build and requires a coil that is roughly 30% smaller (Fig. 1).

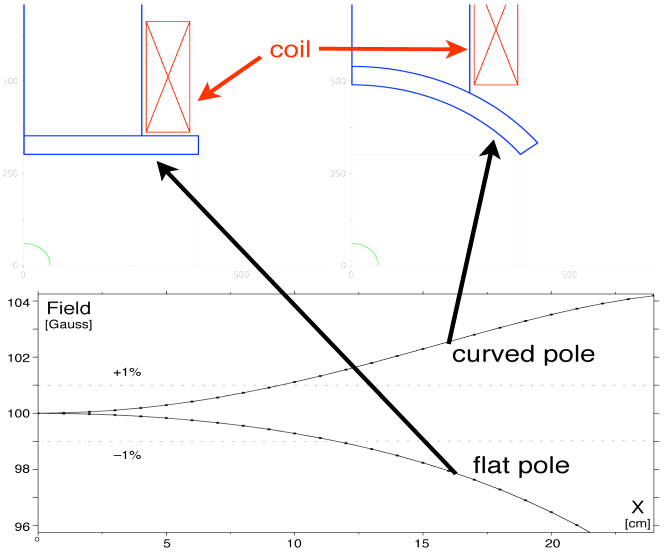

Fig. 1. POISSON models with quarter cross-sections of a magnet with flat and curved poles. The corresponding magnetic field on the mid-plane is shown below. The homogeneity of the field in the 'good field' region (R=60 mm) is within 1% in both cases.

B. Pole Profile Along the Muon Beam

The beam transmission through any ExB cross-field device depends on the matching of electric (E) and magnetic (B) fields in the beam direction. The highest beam transmission will occur in the case of fully matched fields, or in other words when the fields have the same profile. Typically, the electric field has a shorter fringe field extent since the gap between the electrodes is usually smaller than the gap between the magnet poles. The longer magnetic fringe field extent is routinely controlled with field clamping by adding mirror plates at the magnet ends. Additionally, and more significantly, it is beneficial if the magnetic field is also reduced in its middle section as shown in Fig. 2. Such a field reduction in the centre of the magnet can be achieved simply by splitting the magnet poles in halves along the beam direction.

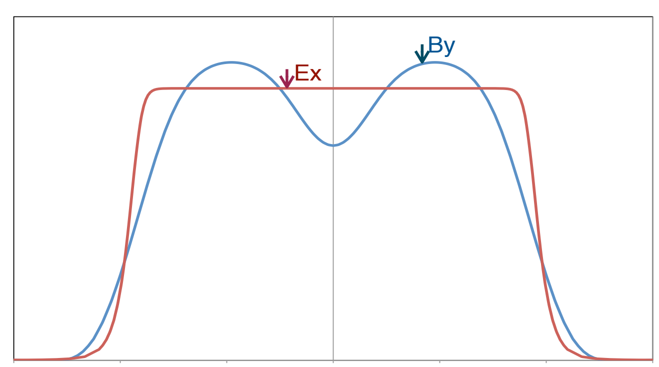

Fig. 2. The electric (Ex component) and magnetic (By component) field profiles in the direction of the beam.

C. Magnet Body Concept

Following the design criteria for the magnet compactness, the idea of integrating the return yoke into the mirror plate was adopted. This increases the thickness of the mirror plates along the beam but still significantly reduces the overall magnet size and weight. Furthermore, accessibility is improved since both magnet sides are completely open and free (Fig. 3).

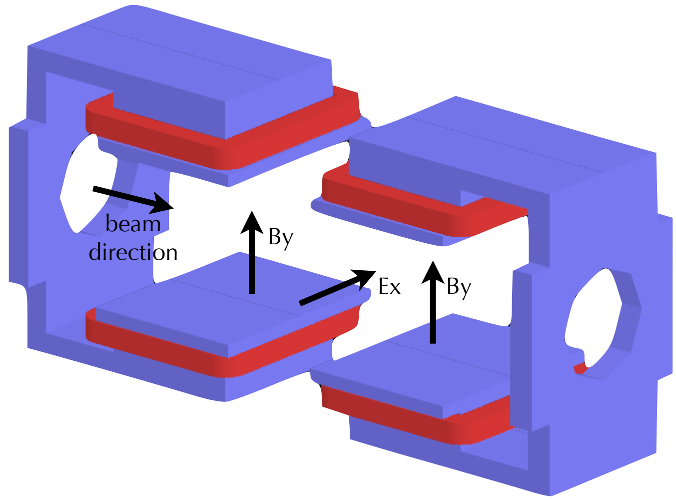

Fig. 3. The conceptual design of the magnet for the spin-rotator device. The device consists of two separate C-shaped dipole magnets, positioned to have the beam travel through a hole in the return yokes. The return yoke also acts as a mirror plate. The E and B-field directions and the beam are perpendicular to each other.

D. Coil

The four coils are of a simple racetrack type. Although the spin-rotator is a low field magnet, due to the large pole gap of 610 mm, the resulting necessary excitation is of 12000 AT/coil. Therefore, a water-cooled coil design was chosen. Assuming one water circuit per coil, the appropriate copper conductor was found to be 8 x 8 mm^2 with a cooling channel of 5 mm diameter. With 69 turns/coil, 1.7 m average length per turn and a nominal current of 180 A, the voltage drop on a coil is just under 10 V. With all four coils in one magnet electrically connected in series, the total voltage drop is under 40 V. This design was chosen to accommodate the existing 200 A/50 V power supply.

E. Optimisation of Magnet Geometry and Analysis

The magnet design was based on calculations and results from TOSCA, a part of the OPERA-3D programme suite for calculating three-dimensional electromagnetic fields [8], as it is evidently a 3D problem. The dimensions and position of the magnet poles and the mirror plates were determined by an iterative optimisation process, controlled with our own program suite OPTIMA [9]. The quality criterion implied on each solution was the amount of deviation of the beam from the spin-rotator central axis. Minimising this deviation assures maximum beam transmission.

The ray-tracing calculations were carried out with the programme TRACK [10], combining the magnetic field from each iterative solution, with the electric field defined by the geometry of the high-voltage electrodes. The final solution resulted in a maximal deviation of the beam of about 2 mm with respect to the magnet central axis (Fig. 4). The horizontal (E-field plane) and vertical (B-field plane) projections of the parallel beam are shown in Fig. 5.

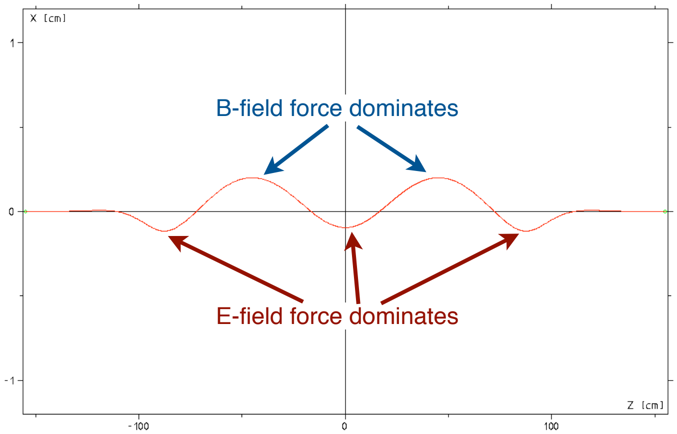

Fig. 4. Well-matched magnetic and electric fields reduce the deviation of the beam axis from the geometrical axis to about 2 mm along the entire beam path, which is small compared to the specified 120 mm aperture.

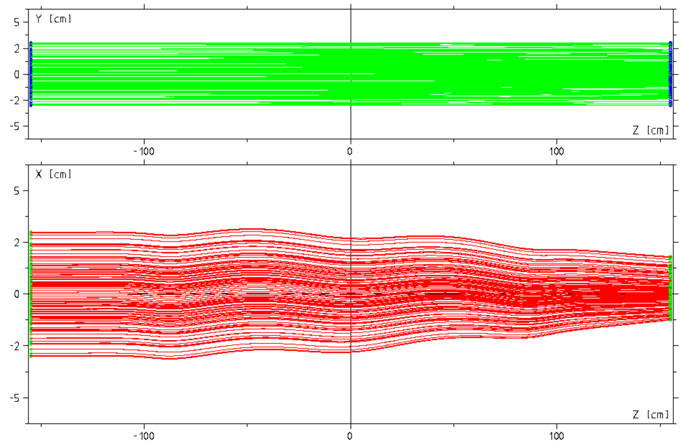

Fig. 5. There is a visible focusing inherent for ExB devices in the plane of the E-field. This is due to the potential difference which accelerates particles on one side of the axis and decelerates particles on the other side, effectively changing the zero net force. The beam shape in the other plane is practically unaltered.

Finally, the designed spin-rotator geometry and the corresponding calculated electric and magnetic field maps were implemented in a simulation program [11] based on GEANT4 [12], [13], using a realistic non-parallel muon beam. The initial muon momentum followed a Gaussian distribution with a mean value of 27.4 MeV/c and a standard deviation of $\sigma_{px}^{entrance} = 0.95$ MeV/c. Also, the spatial distribution in *x* and *y* at the entrance of the spin-rotator were Gaussian-like, with a standard deviation of $\sigma_x^{entrance} = \sigma_y^{entrance} = 25$ mm. The transmission at the end of the spin-rotator predicted by the simulation is 88%. It is interesting to note that unlike in the case of the ideal parallel beam the realistic beam with the finite momentum bite is defocused in the spin-rotator: the resulting deviations are $\sigma_x^{exit} = 37$ mm and $\sigma_y^{exit} = 42$ mm. On the other hand, the standard deviation of the muon momentum is slightly reduced to $\sigma_{px}^{exit} = 0.88$ MeV/c, as muons with a momentum not matching the electromagnetic field are typically stopped in the mirror plate at the exit of the spin-rotator. The overall predicted transmission after two spin-rotators with a refocusing quadrupole triplet in between is ~60%.

III. Construction

For mechanical reasons, the two separate C-shaped dipole magnets comprising the spin-rotator were combined into a single, rectangular structure. Although the central yoke part connecting both dipoles is magnetically inactive as the neighbouring poles lie on the same potential, it simplifies the design and provides structural strength (Fig. 6). In addition, it simplifies the positioning in the beam line, since the two functionally independent C magnets are already aligned with respect to each other. The overall dimensions of the magnet are 2.6 x 1.2 x 0.7 meters and the weight of one complete unit is around 5 tons.

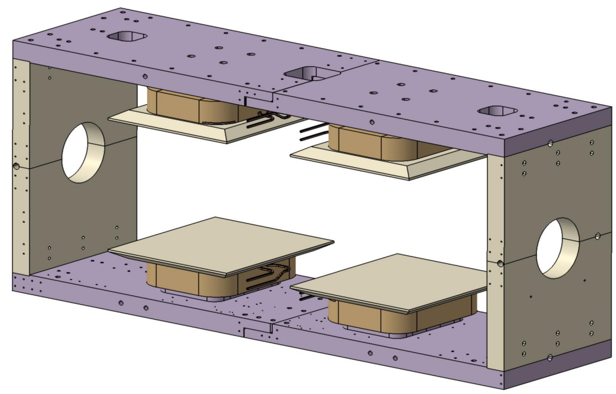

Fig. 6. Two magnetically independent magnet halves are combined in one mechanical unit for structural stability reasons.

To keep the material cost and delivery time within an acceptable range, stock ARMCO sheet metal was chosen. With exception of the pole surfaces (50 mm), all the main panels of the structure were made of 100 mm thick sheets. The central pole body has a dimension of 450 by 320 mm with a thickness of 150 mm; since the 100mm ARMCO sheets are the biggest available size, the pole body had to be divided into several pieces made of the available material sizes. In the end, a vertical separation was chosen to avoid introducing additional air gaps that would disturb magnetic flux (Fig. 7).

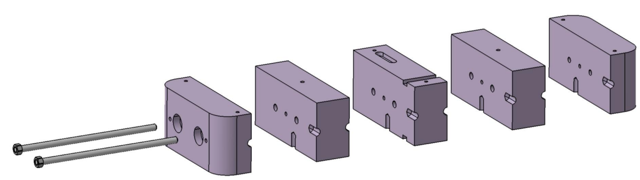

Fig. 7. The pole body is made of 5 separate iron pieces which are assembled together in the way shown here. The corners are rounded to accommodate the coil as close as possible to the pole.

On each mating surface, two precision pins were used to position and constrain the five pole pieces with respect to each other. However, due to the precision manufacturing and subsequent nickel plating, the friction between the individual pieces forming the pole body was lower than expected. This resulted in slight mechanical instabilities since the connecting forces between the pole plate, the main yoke and the pole body are in plane with the mating surfaces of the body pieces; the use of two precision pins was not enough. A third positioning pin or other additional geometrical constraints would have been necessary for this setup. In retrospect, a horizontal (rather than vertical) separation into several pieces would have been mechanically better, even if it could have resulted in a slight performance reduction due to additional air gaps between the individual parts. For the current setup, even with the existing instabilities (resulting in small gaps between the pole body and yoke and pole surface), no influence on the field quality was observed.

IV. Measurements

Both spin-rotator magnets were magnetically measured with a Hall probe (Siemens SBV-585 S1) in our measurement lab. The characteristic excitation curve was calculated from fields on the magnet central axis, measured at discrete currents from –200 A to +200 A and back to –200 A. The full hysteresis curve is symmetrised and reduced to the positive current half in order to cancel out the earth magnetic field. The effective field length curve is shown in Fig. 8, and the deviation of the field from the linearity in Fig. 9.

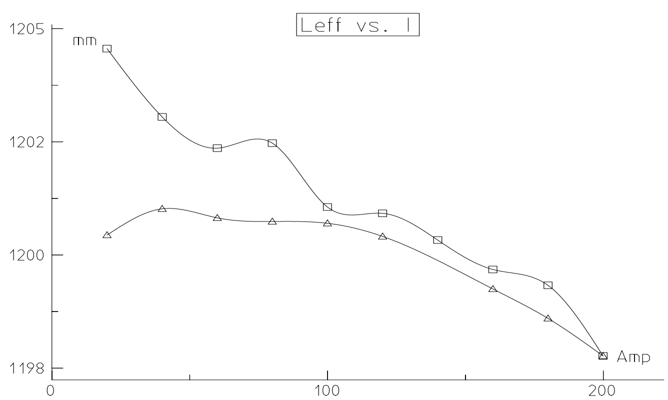

Fig. 8. The magnetic half effective length of the spin-rotator is 1200 mm at the nominal current. This value varies with the current less than 0.2%.

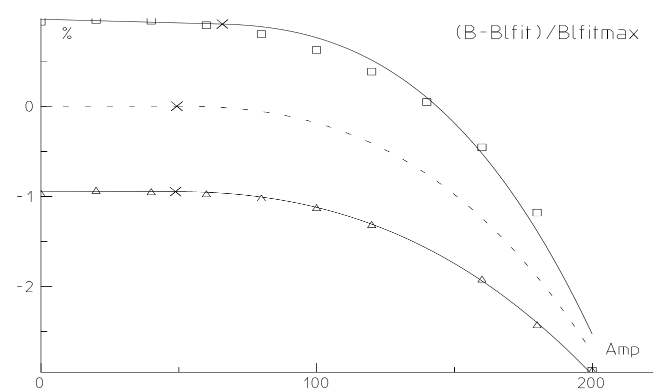

Fig. 9. The graph shows the relative deviation from linearity of the magnetic field at the centre of the spin-rotator. The saturation starts at 50 A and for the maximal current of 200 A it is under 3%. The dotted line represents the averaged fields from magnet ramped down and ramped up.

The magnets were mapped at two currents of 40 A and 175 A. Only the main field component B_y was measured; for beam simulations, the values for the other two components (B_x and B_z) were calculated assuming mid-plane field symmetry. These calculations were based on our standard measurement scheme. To adequately calculate the field nonlinearity, three measuring planes are necessary, one of them being the mid plane. In addition, for each of the two planes above the mid plane, its corresponding symmetrical twin below the mid plane is measured. For each pair of corresponding planes, the average is calculated, cancelling out the influence of the side components on the measured values. This significantly increases the accuracy of calculations of the non-measured field components.

V. Conclusion

The spin-rotator magnet was designed and optimised for high muon beam transmission. The poles are split and the mirror plates are added to achieve a better matching between electric and magnetic fields. The return yokes are integrated into the mirror plates resulting in a very compact magnet, which allows unrestricted access to the high-voltage part of the device.

The measurements of the magnetic fields have shown a very good agreement with those calculated by TOSCA. This is of particular importance in this case, where optimisation was the significant part of the magnet design. No corrections or adjustments after manufacturing and assembly were necessary for both spin-rotator magnets. Although the actually achieved beam transmission rate will be known only when the magnet is brought to operation together with the high-voltage components, the simulations on the measured magnetic field maps indicate a high beam transmission.

Acknowledgment

The authors would like to thank all the people involved in the project that are not mentioned in the authors' list for their contribution, which was as invaluable as ours for the success of the project.

References

[1] A. Yaouanc and P. D. de Réotier, *Muon Spin Rotation, Relaxation, and Resonance: Applications to Condensed Matter,* International Series of Monographs on Physics, Oxford University Press, 2011.
[2] http://lmu.web.psi.ch/facilities/PSI-HighFieldMuSR.html
[3] http://www.oxinst.com/products/low-temperature/Superconducting-magnets/custom-magnets/Pages/custom-magnets.aspx
[4] A. Stoykov, R. Scheuermann, K. Sedlak, "Fast timing detectors for high field µSR spectrometers", *Physica B,* vol. 404, 2009, pp. 990-992.
[5] A. Stoykov, R. Scheuermann, K. Sedlak, "A time-resolution study with a plastic scintillator read out by a Geiger-mode avalanche photodiode", to be published in *Nuclear Instruments and Methods A,* 2011.
[6] http://www.bluefors.com/site/
[7] POISSON/SUPERFISH, Los Alamos National Laboratory, Accelerator Code Group, http://laacg1.lanl.gov/laacg/services/services.phtml
[8] OPERA-3D, Vector Fields Software, Kidlington, UK, http://www.cobham.com/about-cobham/aerospace-and-security/about-us/antenna-systems/kidlington.aspx
[9] V.Vranković, D.C.George, "Smooth shimming of pole profiles", *IEEE Trans. Appl. Supercond.*, vol. 10, 2000, pp. 1372-1375.
[10] V.Vranković, D.C.George, J.M.Schippers, "Ray tracing with the program TRACK (from beam transport magnets to cyclotrons)", XXXIII European Cyclotron Progress Meeting, Warsaw/Kraków, Poland, September 18-21, 2002.
[11] K.Sedlak, R. Scheuermann, T. Shiroka, A. Stoykov, A. R. Raselli, A. Amato, "MusrSim and MusrSimAna - simulation tools for µSR instruments", µSR conference 2011, Cancun, Mexico, to be published in *Physics Procedia*.
[12] S. Agostinelli, *et al.*, *Nuclear Instruments and Methods A,* vol. 506, 2003, pp. 250-303.
[13] J. Allison, *et al.*, *IEEE Trans. Nucl. Sci,* vol. 53, 2006, pp. 270-278.